

# Nutrilyzer: A Mobile System for Characterizing Liquid Food with Photoacoustic Effect

Tauhidur Rahman<sup>1</sup>, Alexander T Adams<sup>1</sup>, Perry Schein<sup>2</sup>, Aadhar Jain<sup>2</sup>, David

Erickson<sup>2</sup>, Tanzeem Choudhury<sup>1</sup>

<sup>1</sup>Information Science, <sup>2</sup>Sibley School of Mechanical and Aerospace Engineering,  
Cornell University

tr266@cornell.edu, ata56@cornell.edu, pms249@cornell.edu, aj329@cornell.edu,  
de54@cornell.edu, tkc28@cornell.edu

## ABSTRACT

In this paper, we propose Nutrilyzer, a novel mobile sensing system for characterizing the nutrients and detecting adulterants in liquid food with the photoacoustic effect. By listening to the sound of the intensity modulated light or electromagnetic wave with different wavelengths, our mobile photoacoustic sensing system captures unique spectra produced by the transmitted and scattered light while passing through various liquid food. As different liquid foods with different chemical compositions yield uniquely different spectral signatures, Nutrilyzer's signal processing and machine learning algorithm learn to map the photoacoustic signature to various liquid food characteristics including nutrients and adulterants. We evaluated Nutrilyzer for milk nutrient prediction (i.e., milk protein) and milk adulterant detection. We have also explored Nutrilyzer for alcohol concentration prediction. The Nutrilyzer mobile system consists of an array of 16 LEDs in ultraviolet, visible and near-infrared region, two piezoelectric sensors and an ARM microcontroller unit, which are designed and fabricated in a printed circuit board and a 3D printed photoacoustic housing.

## CCS Concepts

•Human-centered computing → Ubiquitous and mobile computing systems and tools; •Applied computing → Consumer health;

## Keywords

Photoacoustic Effect, Ubiquitous Material Sensing, Liquid Food Characterization

## 1. INTRODUCTION

Food is a fundamental determinant of our health and wellness. Around the world, we find ourselves facing various chronic diseases and global epidemics including cardiovascular diseases, diabetes, malnutrition or obesity, many of which are predominantly nutrition-related conditions [12]. Moreover, consuming adulterated food can have a disastrous effect on one's health and may lead to serious diseases like cancer, renal failure, loss of vision, etc. In

Permission to make digital or hard copies of part or all of this work for personal or classroom use is granted without fee provided that copies are not made or distributed for profit or commercial advantage and that copies bear this notice and the full citation on the first page. Copyrights for third-party components of this work must be honored. For all other uses, contact the owner/author(s).

*SenSys '16 November 14-16, 2016, Stanford, CA, USA*

© 2016 Copyright held by the owner/author(s).

ACM ISBN 978-1-4503-4263-6/16/11.

DOI: <http://dx.doi.org/10.1145/2994551.2994572>

order to prevent these chronic diseases, ensuring the quality and purity of the food that we consume every day is very important. There are different available techniques to characterize food including Raman, NMR spectroscopy, and mass spectrometry-based technologies [20]. Most of these techniques are typically used in a laboratory environment. The size, cost and the technical skills needed for using such technologies are also prohibitive for a real life application in a mobile environment. A ubiquitous and mobile health technology for characterizing food could have a wide range of applications and could have a significant impact on ensuring food security. Imagine a scenario where a mother goes to the store to pick up milk, she scans the food with her photoacoustics mobile phone case and finds out that there are trace amounts of adulterant in the milk. Similarly, you may want to make sure whether the freshly-squeezed homemade apple juice contains any trace amounts of pesticide, which may come from the residual pesticide on the surface of an apple. An affordable, mobile sensing system, which can characterize nutrients in foods and can detect adulterants, can not only help users to track the quality of the food that they are consuming but also help them to ensure the quality before they purchase the food from the market. Moreover, it can also act as an indirect pressure to the food producers, processors and the distributors in the market to ensure the quality of food. In order to address this, in this study we present Nutrilyzer, a mobile system for characterizing liquid food via the photoacoustic effect.

The photoacoustic (PA) effect is the generation of a sound wave due to the optical absorption in a material sample. This effect was accidentally discovered by Alexander Graham Bell in 1880 while experimenting with long-distance sound transmission [15]. In this experiment, when he exposed a solid sample material with a rapidly interrupted beam of sunlight, an audible sound was produced [16], which was uniquely different for different solid samples due to different optical absorption. As a result, just by listening to the sound wave produced by the photoacoustic effect using light with different wavelengths, it was possible to detect the solid samples. Since the discovery of the photoacoustic effect, this concept has been successfully used for solid, liquid, and gaseous material characterization [24, 45, 44]. Photoacoustic sensing techniques have been explored for various liquid foods and aqueous products characterization [35]. Milk and milk-based product have been extensively studied with photoacoustic spectroscopy using both UV and visible light [32]. The photoacoustic sensing technique was successful at predicting iron content in milk protein concentrate [19] and at detecting whey powder adulterant in skim milk [18].

Although the above-mentioned success of the photoacoustic sensing at liquid food characterization is very encouraging, a traditional photoacoustic setup containing a broadband light source (or a tun-

able laser), a monochromator, a collimator, a chopper, a photoacoustic cell, a highly sensitive acoustic sensor and significant digital signal processing capabilities (a detailed description is given in section 2 and 3) is expensive, bulky, and typically confined to a desktop or benchtop setting. In this study, by replacing the traditional photoacoustic setup with more affordable electronics and fabrication techniques, we developed a mobile and low-cost photoacoustic sensing system, which aims to liberate it from the desktop or benchtop settings. For example, instead of using a highly expensive tunable laser or a bulky broadband lamp with a monochromator, we have used an array of LEDs with different center wavelengths. Similarly, instead of using a chopper to slice the continuous light beam, we used an ARM microcontroller unit and a digital transistor circuit to modulate the LEDs sequentially. Lastly, by replacing the microphone in a hermetically sealed photoacoustic cell, we use a highly sensitive piezoelectric sensor to detect the photoacoustic effect. In section 3, a detailed discussion justifying each of our design choices in this mobile photoacoustic sensing system can be found.

In this paper, we present the design, implementation, and evaluation of Nutrilyzer: a mobile photoacoustic sensing system for characterizing liquid foods. Building on top of the fundamental theory of the photoacoustic effect with a few step-by-step proof-of-concept experiments, we demonstrated how an intensity modulated Light Emitting Diode (LED) can generate the photoacoustic effect on the surface of the electrode of a piezoelectric sensor. We have also illustrated how a piezoelectric sensor can reliably detect and record the photoacoustic signal due to the photoacoustic effect with a high Signal-to-Noise Ratio (SNR). Certain attributes of the photoacoustic signal (e.g., peak-to-peak distance) are not only indicative of the optical absorption at the electrode, but also contain information about the interaction between the light wave and the liquid analyte if the liquid analyte is placed between the LED and the piezoelectric signal. By varying the wavelengths of the light, one could capture the photoacoustic spectra due to the photoacoustic effect by the scattered and transmitted light, which can be used to detect and quantify a certain material in the liquid analyte. This observation is at the heart of Nutrilyzer's implementation. Nutrilyzer uses an array of 16 LEDs with wavelengths in the ultraviolet (UV), visible and near infrared (NIR) range. Using two brass electrode based piezoelectric sensors, Nutrilyzer captures the photoacoustic effect by the scattered and transmitted light. An ARM microcontroller unit modulates the LEDs sequentially and performs the analog-to-digital conversion of the photoacoustic signal. All the circuit in the digital and analog front end are fabricated on a printed circuit board (PCB) and the photoacoustic cell is 3D printed with Polylactic acid (PLA) filament. The photoacoustic cell houses two piezoelectric sensors, the LED array, and the cuvette containing the target analyte liquid food. The two piezoelectric sensors are positioned in the PA cell around the cuvette such that they can capture the photoacoustic signal due to the transmitted and the scattered light. Lastly, by utilizing signal processing and machine learning algorithms, Nutrilyzer maps the unique signature in the photoacoustic spectra at both piezoelectric sensors to various liquid food characteristics including nutrients and adulterants. To evaluate the effectiveness of Nutrilyzer, in this paper, we have developed a model to predict milk protein concentration in whole milk and to detect a few common milk adulterants. We have also developed a model to predict alcohol concentration in clear and colored alcohol.

Specifically, the main contributions of this paper are:

1. Proving the fundamental concept of the theory of photoacoustic effect with step-by-step experimentation.

2. Design and Implementation of a low-cost mobile photoacoustic sensing system, Nutrilyzer.
3. Validation of Nutrilyzer for liquid color dye solution characterization (both classification and concentration prediction).
4. Implementation of the signal processing and machine learning algorithm for liquid food characterization.
5. Evaluation of Nutrilyzer for milk protein concentration, milk adulterants, and alcohol concentration characterization.

## 2. FUNDAMENTALS OF PHOTOACOUSTIC EFFECT

In the year 1880, Alexander Graham Bell discovered the photoacoustic effect as a byproduct of another experiment on long-distance sound transmission [15]. In this experiment, when he exposed a solid sample material with a rapidly interrupted beam of sunlight, a sound was produced [16]. Bell also noticed that the energy of the sound is correlated to the type of solid material and that the sound can be produced by the non-visible portion of the solar spectrum as well. He concluded that this sound is produced by the absorption of the light energy in the solid samples, which lays the foundation of photoacoustic spectroscopy. Around the same time, John Tyndall and Wilhelm Röntgen also found this photoacoustic effect in gas [43, 36]. Although the underlying physics was developed in the 1800s, further explorations into various applications of the photoacoustic effect had to wait for a highly sensitive acoustic sensor (e.g., electret, condenser microphone, piezoelectric sensor) and a light source (e.g., LASER, LEDs). Photoacoustic spectroscopy became more popular when studies demonstrated the sensitivity of this technique in gas detection [44]. It is useful for substances in extremely low concentrations because very strong pulses of light from a laser can be used to increase sensitivity and a very narrow bandwidth can be used for specificity. The first comprehensive theoretical description of the photoacoustic effect in solids was developed by Rosencwaig and Gersho: the so-called RG theory [38]. Now, let us take a better look at the underlying principles behind the photoacoustic effect.

### 2.1 Theory of Photoacoustic Effect

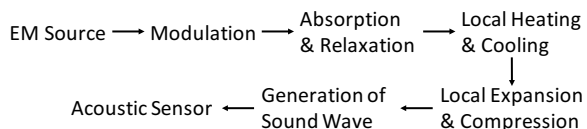


Figure 1: An overview of the generation and capture of photoacoustic signal.

The Photoacoustic (PA) effect is an interesting phenomenon where an acoustic signal is produced by exposing various solid, liquid, and gaseous materials with a modulated light wave. In other simpler terms, it is the sound or acoustic signal produced by a blinking light. The fundamental mechanism behind the generation of the photoacoustic signal is demonstrated in figure 1. The photoacoustic (PA) effect starts with a radiation source of a light or more generally an electromagnetic (EM) wave. When a constant exposure to such a radiation is applied on the surface of a certain material, three processes happen: absorption, reflection, and transmission. In other words, a fraction of the EM radiation gets absorbed by the material. This absorbed energy results in excitation of the molecules, which is followed by non-radiative de-excitation or relaxation processes. The non-radiative de-excitation or relaxation gives rise to

the collisions among molecules and thus an increased thermal activity. Now, instead of a constant intensity exposure if the target material is exposed to a pulsed/modulated radiation of the light (or EM wave), where the intensity of the radiation will change with a certain modulation frequency and pulse width (exposure period), a periodic local heating and cooling is generated within the material. The periodic increase and decrease of temperature in the material lead to a periodic local expansion and compression with the same frequency of modulation. This local change of shape or volume can be sensed by an acoustic sensor (e.g., condenser, electret microphone or piezoelectric sensor).

## 2.2 Piezoelectric Detection of PA Effect

The piezoelectric sensor can quite effectively capture the photoacoustic signal produced by the blinking light due to the photoacoustic effect. A piezoelectric sensor is typically made with a thin layer of elastic material (typically called the electrode) that is attached to a piezoelectric crystal. For example, a brass piezoelectric sensor consists of a thin metal layer of brass and a piezo crystal cut in the shape of a disk [1]. Now, if one applies a modulated or blinking light with a certain wavelength  $\lambda$ , a power  $P$  and a modulation frequency  $\omega$  on the thin layer of metal electrode with a thickness of  $l$ , a photoacoustic signal of  $V_\lambda$  volts will be generated due to the absorption of the light by the brass (as explained in section 2.1).

$$V_\lambda \propto M\alpha_t \frac{1}{l\rho C} \frac{P}{\omega} \quad (1)$$

Here,  $M$  is the coefficient that converts the mechanical strain to voltage,  $\alpha_t$  is the optical absorption coefficient of brass,  $\frac{P}{\omega}$  is the optical energy deposited per cycle on the brass layer,  $\frac{1}{l\rho C}$  captures the material characteristic of brass that determines the heat generation on the brass layer. A detailed theoretical derivation of this equation can be found in the work by Jackson and Amer [26]. Equation 1 demonstrates that the total energy of the acoustic signal ( $V_\lambda$ ) captured by the sensor is proportional to the optical absorption coefficient ( $\alpha_t$ ) by the material of the electrode. The total energy of the photoacoustic signal is also dependent on the wavelength of the EM wave as different wavelength of EM wave is absorbed by the electrode material differently. Equation 1 also emphasizes that by maximizing the deposition of the modulated optical radiation, by selecting a material with high optical absorption and good thermoelastic properties as the electrode, by reducing the thickness, one could maximize the photoacoustic signal detected by the piezoelectric sensor due to photoacoustic effect. In section 4, we present the proof-of-concept experiments of photoacoustic effect with a blinking LED and a brass piezoelectric sensor where we will experimentally verify this theoretical model in equation 1.

By capturing the photoacoustic effect on the electrode of a piezoelectric sensor with an array of blinking light sources at wavelengths ( $\lambda_1, \lambda_2, \dots, \lambda_N$ ) for a certain number of blink-periods, we can record  $N$  photoacoustic time series ( $V_{\lambda_1}(t), V_{\lambda_2}(t), \dots, V_{\lambda_N}(t)$ ). By estimating the photoacoustic amplitudes from the raw time series at all the  $N$  wavelengths, we can measure the photoacoustic spectra [amplitudePA $_{\lambda_1}$ , amplitudePA $_{\lambda_2}$ , ... amplitudePA $_{\lambda_N}$ ]. In section 4, we will present the detailed signal processing steps for the conversion from  $V_{\lambda_n}(t)$  to amplitudePA $_{\lambda_n}$ . Between the creation of the intensity modulated light wave of a certain wavelength at the blinking light source and the generation of photoacoustic wave, the light wave interacts with the medium along its path length and the electrode material of the piezo. The light passing medium could absorb, scatter the light and thus could effect the transmission of the light on the surface of the piezo electrode, which would affect the PA spectra. Essentially, the PA spectra con-

tain rich information about how the light wave of a certain wavelength, after its creation at the blinking light source, is treated by the medium and the electrode material. As a result, if we place the liquid analyte between the light source and the piezo electrode as the medium, the recorded PA spectra will not only capture the optical absorption by the electrode material but also capture the optical filtering by the liquid analyte. On the other hand, if we do not place the liquid analyte between the light source and the piezo electrode as the medium, the recorded PA spectra will only capture the optical absorption by the electrode material. By carefully filtering the PA spectra with the liquid analyte from that of without liquid analyte, we can capture the analyte liquid's transmission and scattering characteristics. In this study, we use the analyte liquid food's transmission and scattering characteristics in the form of the PA spectra, to model various nutrients (or more generally chemical compounds) in the liquid food. We will present a detailed discussion on how we extract the transmission and the scattering characteristic of the analyte liquid food in section 6.

## 3. DESIGN CONSIDERATIONS

In order to bridge the gap between the fundamental physics of photoacoustics to the development of a mobile photoacoustic sensing system, we analyze a few design criteria including the excitation source, wavelength tuning, intensity modulation, acoustic signal capture, and photoacoustic cell design.

### 3.1 Excitation Source and Wavelength Tuning

The type of excitation source is one of the most important design considerations for our system. The signal-to-noise ratio of the photoacoustic signal increases with the luminescence of the light source. As a result, the light source needs to be relatively bright. In order to capture the photoacoustic signal across multiple wavelengths, we also need to select a particular wavelength with a bandwidth as narrow as possible. Traditionally, high power broadband light source (e.g., Argon or Xenon lamp) is used in conjunction with a collimator and a monochromator [37]. While a collimator increases the brightness of the light by focusing it, a monochromator selects a narrow band light with a certain center wavelength. Another alternative is the traditional tunable Q-switched Nd:YAG pumped OPO, Ti:sapphire or dye laser system [24]. However, both of these setups are bulky and expensive. They are typically implemented in a desktop or benchtop settings, which is not desirable for designing a compact, portable and cheap mobile system. To facilitate the translation of photoacoustic sensing system from laboratory to mobile settings, we need to use a cheaper and more compact excitation source. Pulsed laser diodes have been explored as an excitation source for different biomedical imaging applications [14, 27]. Although pulsed laser diodes are compact and relatively inexpensive (typically about \$100 USD), the major drawback is that the pulsed laser diodes come with a limited range of wavelengths to select from. Another problem is that it requires more sophisticated (and expensive) acoustic sensing and capture. Although pulsed laser diode has a modulation frequency in the range of a few Hz, the pulse width is typically in the range of a few nanoseconds. The nanosecond-range pulse width further increases the complexity of the acoustic sensor or microphone. Due to this short pulse width, the pressure wave can only be sensed and digitized by a highly sensitive ultrasonic microphone and an Analog-to-Digital Conversion (ADC) with a sampling rate in the ultrasonic range.

As an excitation source, Light Emitting Diodes (LEDs) have several advantages over pulsed laser diodes [13]. The LED is a very cheap (typically < 10 USD) continuous wave light source available with a wide range of center wavelengths from UV, visible, near

and mid-infrared regions. The high peak power LEDs can easily meet the high optical energy/brightness requirement of a photoacoustic excitation source. Unlike the pulsed laser diodes, which emit highly focused and collimated light, LED typically emits diffuse light over its angle of operation. An optical lens can easily correct this shortcoming by focusing the LED light. As every LED comes with a particular center wavelength, we need to use an array of LEDs to capture the spectrum across multiple wavelengths. Due to the small form factor of surface mounted LEDs available in the market, one could quite easily put an array of LEDs in a small Printed Circuit Board (PCB). Considering all these factors we have decided to use an array of high peak power LEDs (forward current of about 180 mA) is used in this study.

### 3.2 Intensity Modulation

In our LED array (excitation source), the intensity of each LED needs to be separately modulated with a certain modulation frequency and pulse width. Traditionally, mechanical choppers (a fan with blades) were used to slice the continuous wave light source [37]. However, it is bulky and noisy, which degrades the signal-to-noise ratio (SNR) of the photoacoustic signal. An alternative approach could be to use a transistor as a switch to turn the LEDs on and off digitally. In order to maintain a constant forward current through all the LEDs with different rated forward voltages, we power each LED by a constant current DC/DC Buck LED driver [8]. As a result, the brightness or luminance of the LEDs remains constant and robust against subtle voltage changes of the battery. By toggling a control digital pin in the LED driver, one can blink or modulate the LED's intensity.

### 3.3 Capturing Photoacoustic Signal

Capturing the photoacoustic signal requires a sensitive acoustic sensor (e.g., electret microphones, piezoelectric sensors) in the infrasonic range. As a low modulation frequency ( $< 20$  Hz) is typically used for reliable capture of the photoacoustic signal with a high SNR. Traditionally, the photoacoustic signal, which is produced due to the optical absorption and non-radiative de-excitation of a material, is captured by electret or MEMS microphone in a hermetically isolated photoacoustic cell filled with nonabsorbing gas and the target analyte. As the intensity modulated light falls on the target condensed analyte, heat and pressure waves are generated, which gets transferred to the gas. With an electret or a MEMS microphone placed inside the photoacoustic cell, we can measure the pressure change in the gas. However, the major drawback of this approach, especially in a mobile setting, is that it requires sophisticated and bulky air-tight and gas-filled photoacoustic cell with analyte material transport mechanism. Considering all these factors in this study, we have used a brass piezoelectric sensor [1] to capture the photoacoustic effect. As mentioned earlier, the intensity modulated LED gives rise to a local contraction and expansion on the surface of the piezoelectric sensor's electrode, which can easily be recorded by the piezoelectric sensor.

## 4. PROOF-OF-CONCEPT OF PA EFFECT: WITH A SINGLE LED

In this section, we outline a few proof of concept laboratory experiments of PA effect using a single excitation source with a LED. With the step-by-step experimentations, we explored the generation with an intensity modulated high power LED and the piezoelectric capture of the photoacoustic signal. We have also explored the effect of various setup parameters on the PA signal amplitude including the intensity of the LED, modulation frequency, pulse

width, and the material characteristics of the piezoelectric transducer's electrode.

### 4.1 Generation and Capture of Photoacoustic Signal

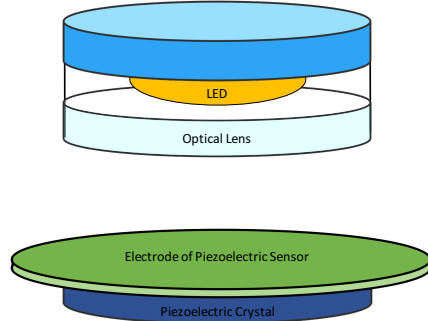


Figure 2: The experimental setup of generation and capture of photoacoustic signal.

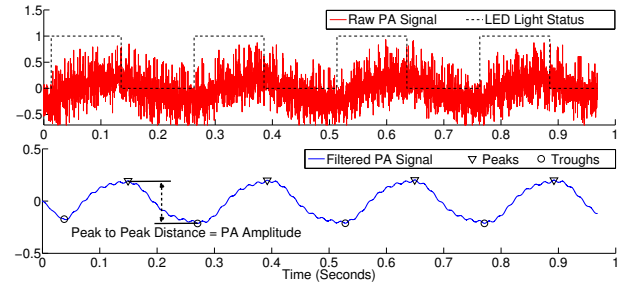


Figure 3: The top subplot shows Generation of raw PA signal with the setup shown in figure 2. The bottom subplot shows the filtered PA signal and how to estimate PA amplitude.

We have built a simple photoacoustic setup consisting of an LED, an optical lens, and a piezoelectric sensor, as demonstrated in figure 2. The LED (Center wavelength of 448 nm, LUXEON Rebel and LUXEON Rebel ES Colors [4]) is directly attached to an optical lens via a lens tube to collimate and focus the light beam on the metal plate. The peak forward voltage and current were set to be respectively 3.3V and 180 mA. We set the distance between the light source and the metal plate to be 20 mm. As the light beam falls on the piezoelectric sensor's brass electrode, the temperature of the illuminated metal surface increases due to optical absorption. It leads to a local expansion of the region. Similarly, in the absence of light, the metal surface cools down and contracts. As the LED is periodically blinked with a certain modulation frequency, the repeated contraction and expansion can be sensed by the piezoelectric crystal. A detailed and systematic mathematical derivation of the photoacoustic signal generation on a metal surface with a piezoelectric signal can be found in [26]. Figure 3 shows the generation of the PA signal by a modulating LED with a frequency of 4 Hz and a pulse width of 50% using the setup in figure 2. The top subplot in figure 3 shows the noisy raw PA signal that was captured with a Tektronix TDS2024C Oscilloscope. When the LED goes from 0 (off) to 1 (on), the raw PA signal increases. Similarly, the raw PA signal decreases, as the LED goes from 1 (on) to 0 (off). Also, notice that the raw PA signal contains a lot of noise. With a simple moving average filter, we can get rid of most of the high-frequency

noises from the raw signal, as can be seen in the bottom subplot in figure 3. Lastly, the distance between the peaks and troughs of the filtered PA signal is used to measure the PA amplitude. The median of the PA amplitudes (peak to peak distances) over multiple periods of LED blinks can estimate the optical absorption of the brass surface of the piezoelectric sensor with respect to the center wavelength of the LED. Later in section 6.1, we will use multiple LEDs (array of LEDs) to estimate the photoacoustic signals for multiple wavelengths, which we call photoacoustic spectra.

## 4.2 Effect of Setup Parameters on PA Signal

In this section 4.2, we will analyze how various photoacoustic setup parameters (e.g., forward current of the LED, modulation frequency, pulse width and thickness of the metal plate) affect the PA signal generation and capture.

### 4.2.1 Input Power

| $I_{forward}$ (mA) | 70   | 90   | 130  | 180  | 240  | 270  |
|--------------------|------|------|------|------|------|------|
| PA Ampl (V)        | 0.66 | 0.74 | 0.92 | 1.44 | 1.70 | 1.84 |

Table 1: With the increase of forward current  $I_{forward}$  through the LED, the PA signal amplitude increases.

Forward current through the LED determines the brightness or luminance of the excitation source. As can be seen in Table 1, the peak-to-peak distance or amplitude of the PA signal increases with the increase of the forward current  $I_{forward}$ . As the excitation source becomes brighter, the optical absorption in the metal surface also increases. The temperature rise on the surface of the piezoelectric sensor's metal electrode forces it to bend more, which results in a higher PA signal amplitude captured by the piezoelectric sensor. This result confirms the piezoelectric detection model in equation 1 that the PA signal  $V_\lambda$  is proportional to the optical power of LED  $P$ .

### 4.2.2 Modulation Frequency

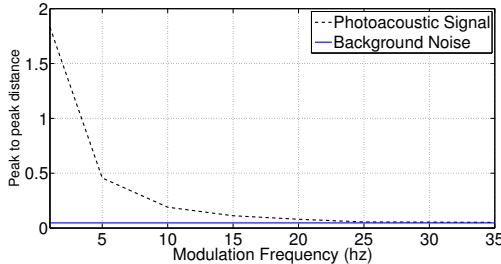


Figure 4: With the increase of modulation frequency the signal-to-noise ratio of the PA signal diminishes.

The modulation frequency plays a very important role in generating the PA signal. With a low modulation frequency, the light beam from the LED can excite the transducers electrode (brass disk) for a longer period of allowing the disk to expand and bend more. As a result for low modulation frequency, the PA amplitude is high. With the increase of the modulation frequency, the PA amplitude decreases. As can be seen in figure 4, between 1 Hz and 10 Hz the amplitude of the PA signal was significantly higher than that of the background noise. Once the modulation frequency increases beyond 10 Hz, the SNR drops very quickly until the PA signal is

lost in the background noise at around 20 Hz. This result confirms the piezoelectric detection model in equation 1 that the PA signal  $V_\lambda$  is inversely proportional to the modulation frequency  $\omega$ .

### 4.2.3 Pulse Width

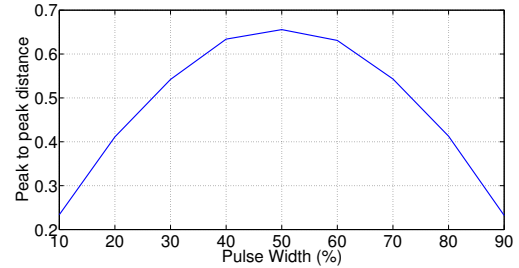


Figure 5: The intensity modulated light with 50% pulse width yields the PA signal with the highest amplitude.

Pulse width or duration is the percentage of time in a period when the LED is on. As can be seen in figure 5, pulse width plays a major role in determining the PA signal amplitude. With very low or very high pulse width, we fail to achieve a high amplitude PA signal. At a pulse width lower than 50%, the electrode gets smaller amount of light to absorb, which results in a smaller expansion. On the other hand, at a pulse width higher than 50%, the electrode does not get enough time for compression, which also leads to a smaller PA signal. As a result, at 50% pulse width, the peak-to-peak distance of the PA signal is at its maximum.

### 4.2.4 Diameter of Piezoelectric Transducer

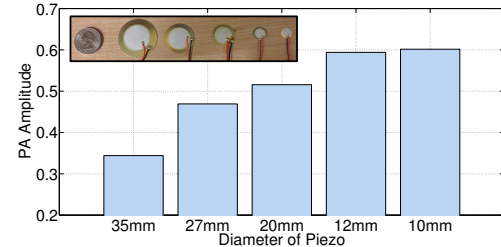


Figure 6: As the diameter of a piezoelectric disk gets smaller, it yields higher PA response.

A piezoelectric transducer consists of an electrode, in this case, a brass metal disk, and a piezoelectric ceramic crystal disk. It comes in different diameters. In order to select the optimal diameter that maximizes the photoacoustic signal strength, we compared the PA amplitude produced by piezoelectric sensors with 5 different diameters using the same setup shown in figure 2. As can be seen in figure 6, with the decrease of the piezoelectric sensor's diameter the PA amplitude increases. This can be quite easily explained by the fact that smaller plate is easier to bend by the optical absorption due to the PA effect. The larger plate on the other hand is more difficult to bend due to its inertia, which leads to the decrease in the PA signal amplitude. In fact, the same phenomenon can be observed if we add more mass to the surface of the electrode on the piezoelectric transducer. In order to explore this effect, we increasingly added thin layers of copper tape (thickness of one layer is 0.085mm) to the outer surface of the brass electrode on the transducer. the PA amplitude drops (as can be seen in figure 7), which is

also observed by other recent studies on photoacoustics [26]. This result confirms the piezoelectric detection model in equation 1 that the PA signal  $V_\lambda$  is inversely proportional to the thickness of the electrode  $l$ .

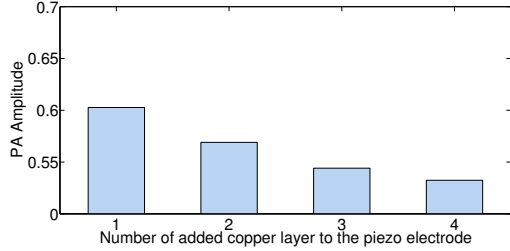


Figure 7: The PA amplitude decreases with added mass to the electrode of piezoelectric transducer.

#### 4.2.5 Material Characteristics of Piezo Electrode

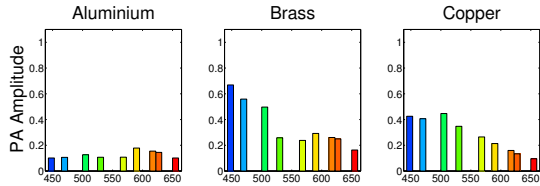


Figure 8: Different types of solid materials in the outer surface of the piezo electrode produced different PA amplitude at different wavelengths. Brass was the most sensitive to the majority of the wavelengths of LED light.

In order to explore whether and how the material characteristics of the electrode affect the PA signal, we have attached different materials (aluminum, brass, copper) to the transducers electrode. Figure 8 illustrates the PA amplitude produced by 9 different LEDs with varying center wavelength in the visible spectrum. The three materials produced varying PA amplitudes at different wavelengths due those three material's unique optical absorption properties. This confirms the piezoelectric detection model presented in equation 1 in section 2.2 that the material characteristics of the piezo electrode affects the PA signal generation. In this study, we have selected brass, as it was overall the most sensitive to the majority of the wavelengths.

From all the above-mentioned experiments, we have learned how to select the input power of the LED, modulation frequency, pulse width, piezoelectric transducer diameter in order to maximize the signal strength of the PA signal, which confirms the piezoelectric detection model presented in equation 1 in section 2.2. We will use a high power LED with high forward current and luminous intensity. As the forward current affects the PA amplitude significantly, it is also very important to drive the LED with a constant current source. The PA signal amplitude has an inverse relationship with the modulation frequency. As a result, we want to use a moderately low modulation frequency with 50% pulse width to generate the photoacoustic signal. Lastly, we use the thin and small brass disk as the piezoelectric sensor's electrode to maximize the PA response.

## 5. MOBILE SYSTEM IMPLEMENTATION

Design and implementation of a mobile photoacoustic sensing system is a major challenge that we addressed in this study. Fig-

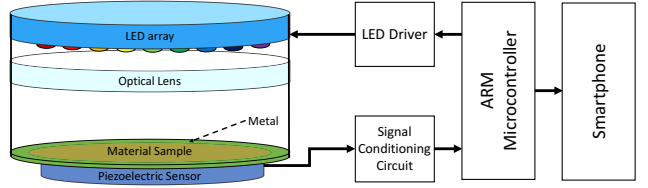


Figure 9: The functional block diagram of the proposed mobile photoacoustic sensing system, Nutrilyzer.

ure 9 is a high-level functional block diagram of the proposed mobile photoacoustic sensing system, Nutrilyzer. In what follows, we present a detailed description of all the functional blocks.

### 5.1 ARM Microcontroller

The ARM-microcontroller (commercial name Teensy 3.1 [10]), which is at the heart of the mobile system, has three major responsibilities. Firstly, it interacts with the constant current Buck LED driver to control the LED array (excitation source). The ARM microcontroller modulates the intensity of each LED separately with a certain modulation frequency. Each LED in the array is blinked for a predefined number of periods until it moves to the next LED. Secondly, while the LEDs are intensity modulated, the internal ADC of the microcontroller converts the analog, amplified and filtered PA signal to a digital signal. Lastly, after the analog to digital conversion and preprocessing, it passes the data to the phone for running further signal processing, machine learning (ML) algorithms and for displaying the results. We use the microcontroller's internal ADC for converting the output analog signal from the signal conditioning circuit to a 16-bit digital signal with a sampling frequency of 1000 Hz. As the low modulation frequency signal generates infrasonic PA signal (less than 20 Hz), our sampling frequency of 1000 Hz satisfies the Nyquist criteria.

### 5.2 LED Array and Driver

We have designed a LED array containing 16 LEDs with center wavelengths in the ultraviolet (UV), visible and near-infrared (NIR) range. Table 2 lists all the 16 LEDs with their respective color, center wavelength  $\lambda$  and forward current rating  $I_f$ . We know from section 4.2 that the PA amplitude increases with the increase of radiant power, which is typically proportional to the rated forward current. As a result, we have chosen a set of relatively high power LEDs in the UV, visible and near-infrared (NIR) range with rated forward current from 100 to 1000 mA. The power rating of the LEDs will primarily determine the total power consumption of our Nutrilyzer system. As a result, LEDs that generates high irradiance with less forward current will certainly enhance the power efficiency of the overall system. Luxeon Rebel, Luxeon Rebel ES Colors and Luxeon Z color line offers a set of visible light high power LEDs that meets our requirements [4, 3, 5]. Most of the off-the-shelf UV LEDs come with a low power setting. However, we have selected two UV LEDs [6] from Luxeon Z UV line with center wavelengths of 385 and 395 nm. Lastly, we have included four LEDs with center wavelengths in the NIR range (respectively, 745, 830, 850 and 940 nm).

In order to capture the PA amplitude with all these LEDs, each LED is separately modulated or blinked 15 times before it goes to the next LED. As the LEDs' forward current rating is relatively high and the ARM microcontroller's pin out can not supply high current, each LED in the LED array is separately powered by a

| Ind | Part Num       | Color      | $\lambda$ (nm) | $I_f$ (mA) |
|-----|----------------|------------|----------------|------------|
| 1   | LHUV 0385 [6]  | UV         | 385            | 500        |
| 2   | LHUV 0395 [6]  | UV         | 395            | 500        |
| 3   | PR01 0500 [4]  | Royal Blue | 448            | 1000       |
| 4   | PB01 0040 [4]  | Blue       | 470            | 1000       |
| 5   | PE01 0050 [4]  | Cyan       | 505            | 1000       |
| 6   | PM01 0090 [4]  | Green      | 530            | 1000       |
| 7   | LXZ1 PX01 [5]  | Lime       | 568            | 1000       |
| 8   | PL01 0060 [4]  | Amber      | 590            | 700        |
| 9   | LXM3 PW71 [3]  | White      | -              | 700        |
| 10  | PH01 0060 [4]  | Red Orange | 617            | 700        |
| 11  | PD01 0050 [4]  | Red        | 627            | 700        |
| 12  | LXM3 PD01 [4]  | Deep Red   | 655            | 700        |
| 13  | ELSH Q61F1     | NIR        | 745            | 100        |
| 14  | VSMF 2700 GS08 | NIR        | 830            | 100        |
| 15  | VSMY 2850 RG   | NIR        | 850            | 100        |
| 16  | SFH 4441       | NIR        | 940            | 100        |

Table 2: The part number, color, wavelength and rated forward current of the LEDs in our LED array.

constant current DC/DC Buck LED driver [8], which is connected to a 8 volt DC supply. Essentially the LED driver converts the DC power source to a constant current supply of 180 mA. The LED driver also allows us to modulate the intensity of each LED individually. We use a modulation frequency of 2 Hz and a pulse width of 50%, as discussed in section 4.2.2 and 4.2.3

### 5.3 Piezoelectric Sensor and Signal Conditioning

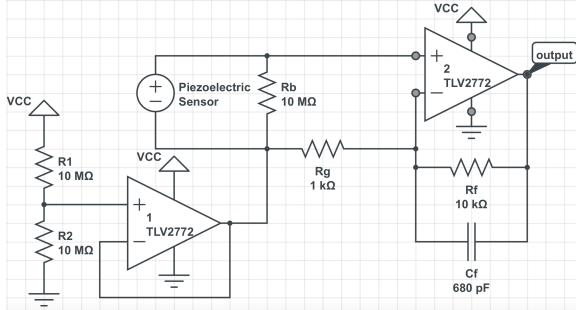


Figure 10: Opamp-based signal conditioning circuit.

The piezoelectric sensor (Brass piezo disk sensors [1]) generates a very low voltage signal in response to the PA effect. Moreover, the piezoelectric sensor has a much higher output impedance than the input impedance of the analog input pin of the ARM microcontroller. As a result, the raw PA signal needs proper signal conditioning (i.e., amplification and impedance matching) before the analog pin of the ARM microcontroller can run the analog-to-digital conversion. Our opamp-based signal conditioning circuit (in figure 10) addresses these issues. Because of the high impedance of the piezoelectric sensor, we used a high-input impedance JFET or CMOS input opamp. In this particular implementation, we have used a CMOS Rail-to-Rail operational amplifier TLV2772 [2]. By using the appropriate values of  $R_b$ ,  $R_f$ ,  $R_g$  and  $C_f$  (as shown in figure 10), we amplify the weak raw PA signal by a factor of 11. We supply a regulated 3.3 Volts to the  $V_{CC}$  of the opamp. Lastly, to shift the amplified and signal conditioned PA signal within the dynamic range of the ADC of the microcontroller, we provide an additional  $V_{CC}/2$  from the first opamp's output to the second opamp's circuit. The output of the opamp circuit is connected to an analog pin

of the microcontroller for analog-to-digital conversion.

### 5.4 Photoacoustic Cell

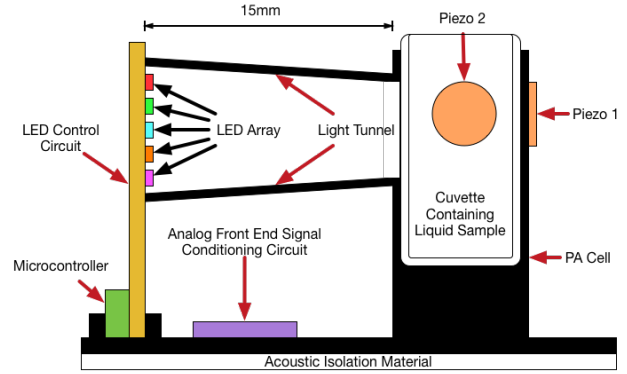


Figure 11: The side view of the photoacoustic cell.

The photoacoustic cell consists of a piezoelectric sensor, optical lens, the target analyte material, and a 3D printed light tunnel that encapsulates the LED array to prevent external light from influencing the PA signal and prevents the light from hitting anything other than the target analyte material (figure 11). The dimension of the PA cell is respectively 12 x 12 x 40 mm. The inside of the cell is spray-painted matte black so that the wall of the PA cell equally absorbs all the different wavelengths emitted by the LED array. We use cuvette as a container for the analyte liquid. We used a UV grade cuvette that allows light in UV, visible and NIR to pass through it. The volume and path length of the cuvette was 4.5 ml and 10 mm. The inner dimension of the PA cell was designed such that it will hold the cuvette in a firm and stable manner. Once the target material is deposited in the cuvette to be analyzed, we place the cuvette inside the PA cell. The PA cell is closed so that no external light can get into the cell. In order to prevent external sound/vibrations from introducing noise into the PA signal, we attached layers of soft silicone rubber to the bottom of the PA cell to provide acoustic isolation for the piezoelectric sensors. As can be seen in figure 11, the PA cell also holds two piezoelectric sensors. Piezo 1 is placed facing the LED array, while Piezo 2 is perpendicular to Piezo 1. Piezo 1 is positioned such that it can capture the PA signal by the transmitted light, while Piezo 2 is positioned to capture the PA signal of the scattered light by the analyte liquid solution. We will talk about the functionalities of the Piezo 1 and Piezo 2 in a more detailed manner in section 6.

### 5.5 Fabrication and Design

To build a robust, mobile PA system, we used several different materials and fabrication and design techniques. The LED array and driver circuit were fabricated in-house with our PCB milling machine on a 1 oz copper clad FR4 double-sided board. Figure 12 illustrates all the electronic components. The main board contains the LED array, an array of LED drivers and the ARM microcontroller. We have a separate board that contains the analog front end signal conditioning circuit for the piezoelectric sensors (Piezo 1 and Piezo 2). These boards are connected with each other by ribbon cables. Lastly, the system is powered by 3 LiPo batteries connected in series. The light tunnel and housing, which holds the microcontroller, LED array, LED drivers, signal conditioning circuit, and photoacoustic cell were 3D printed using Polylactic acid (PLA) filament. It was spray-painted matte black and mounted on

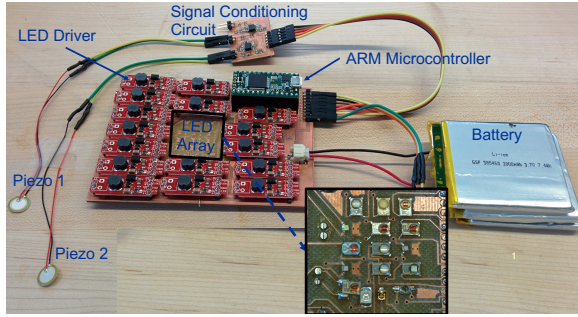


Figure 12: All the electronic components used in our photoacoustic sensing system.

top of soft silicone rubber for acoustic isolation. Figure 13 shows the front view of our proposed PA sensing system, Nutrilyzer.

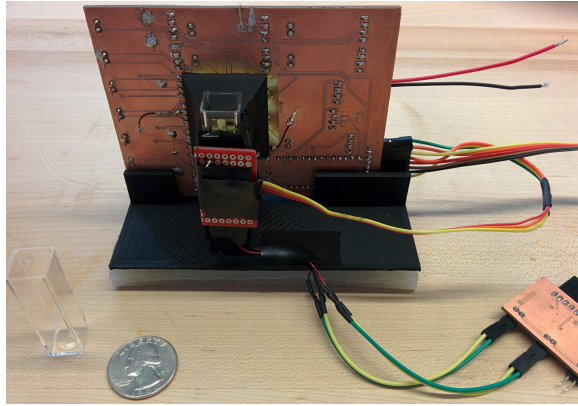


Figure 13: Front view of our PA sensing system with electronics mounted in housing.

## 6. CHARACTERIZING COLORS WITH NUTRILYZER

In this section, we put our proposed Nutrilyzer system to test. As the first proof-of-concept experiment with the full Nutrilyzer system, we explore whether we can at first classify the colors of different color dye solution in water. Later, we estimated the predictability of the color dye concentration in dye-water solutions.

### 6.1 Classifying Color Dye-Water Solutions

As the LEDs are sequentially intensity modulated or blinked, the light beam transmits through the light tunnel, the analyte solution in the cuvette and the wall of the cuvette before it hits the metal plate surface of Piezo 1 sitting diagonally across the LED array. As the light beam tries to penetrate through the analyte liquid solution, some part of the light beam also gets scattered and hits the Piezo 2, which is in the side wall of our PA cell (as explained in section 5.4). The top plot in subfigure 14a shows the PA signal of the Piezo 1, while the top plot in figure 14b shows the PA signal of the Piezo 2. In order to estimate the PA spectra of both Piezo 1 and Piezo 2, we at first estimate the peaks and troughs of the PA signals. Then we estimate the running peak to peak distance (the distance between consecutive peak and trough), which we call PA amplitude. The bottom plot in subfigure 14a and 14b shows the running PA amplitude over time. In these two subfigures, we can also observe

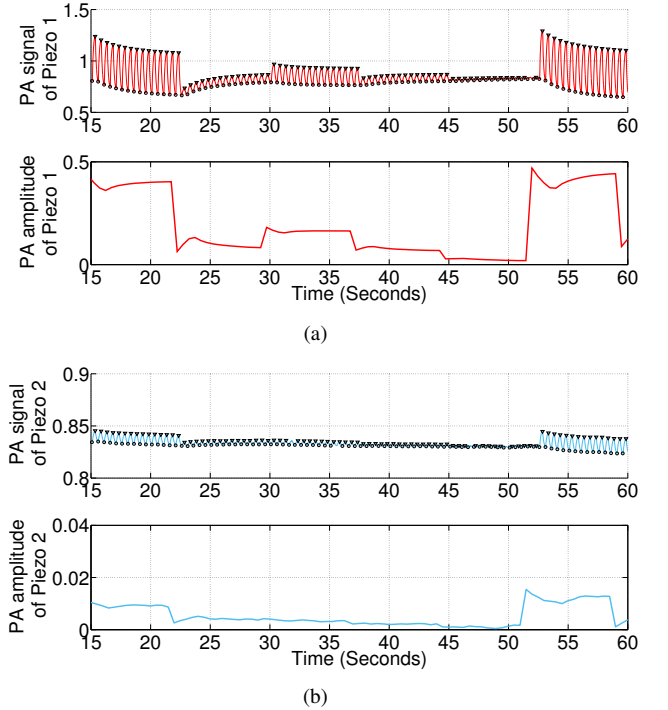


Figure 14: demonstrates how the PA signal is produced by the intensity modulated LEDs and how we process the PA signal and estimate the PA spectra from both (a) piezo 1 and (b) piezo 2. Top subfigure of both (a) and (b) shows the peaks and troughs of the filtered PA signal. Bottom subfigure of both a and b shows the PA amplitude or distance between the peaks and troughs of the PA signal over time.

a distinct transient response in the running PA amplitude of both Piezo 1 and 2. This transient response is marked by an overshoot or an undershoot in the PA amplitude while moving between two consecutive LEDs (Every LED is blinked 15 times). This transient response happens only for a few periods of blinks until the amplitude of the PA signal reaches its steady state. By estimating the median of the PA amplitude values estimated across the duration of each LED, we can avoid the transient PA amplitude values and can robustly estimate the true PA amplitude of Piezo 1 and 2 individually. Thus by measuring the median value of PA amplitude values of Piezo 1 and 2 for each LED separately, we can estimate the PA spectra of both Piezo 1 and 2 across all the wavelengths (or LEDs). Lastly, we normalize the spectra with respect to the PA spectra recorded with an empty cuvette in the system. If the PA amplitude or peak-to-peak distance of target analyte liquid solution and the empty cuvette in  $\lambda$  wavelength is respectively  $amplitudePA(\lambda)$  and  $amplitudePA_{EmptyCuvette}(\lambda)$ , using equation 2 we can estimate the normalized PA spectra.

$$NormalizedPAS = \frac{amplitudePA(\lambda)}{amplitudePA_{EmptyCuvette}(\lambda)} \quad (2)$$

By comparing the PA amplitudes for different LEDs (or at different wavelengths) of Piezo 1 (in figure 14a) and Piezo 2 (in figure 14b), one could easily notice that the PA amplitudes are different in both magnitude and pattern. For example, the PA amplitudes of Piezo 1 for different LEDs are much higher in magnitude than that of Piezo 2. Moreover, the PA amplitude of Piezo 1 for the third

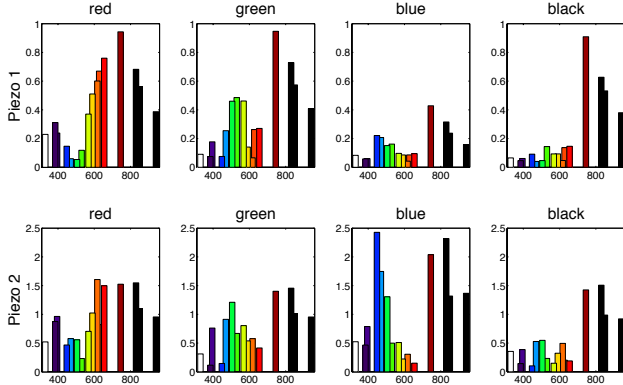


Figure 15: Normalized Photoacoustic Spectra of different color dye-water solutions. Each bar represents the normalized PA amplitude by a particular LED with a certain center frequency.

LED captures a much stronger response than that of the two neighboring LEDs (i.e., second and fourth LED in figure 14). The Piezo 1 captures the transmitted light, while the Piezo 2 is positioned to get the scattered light. As a result, the PA amplitudes of the Piezo 1 and 2 are respectively due to the transmitted and scattered light. For a certain wavelength of light, a particular analyte liquid solution may appear to be transparent and may allow a higher light transmittance, which would give rise to a higher PA amplitude of Piezo 1. For some other wavelength, the analyte liquid solution may be relatively opaque, which in turn may give rise to a higher amount of scattered light. The higher level of scattering would give rise to a higher PA amplitude of Piezo 2. Thus, theoretically, the PA spectra of Piezo 1 and 2 contains a lot of complementary information about the target liquid solution, which could help to characterize different material properties of the liquid. In section 6.2 with the help of some experimental result we will illustrate how with these two piezoelectric sensor captures transmitted and scattered light separately and how the PA amplitudes from these two piezoelectric sensors contain complementary information about the liquid analyte.

Figure 15 shows the normalized photoacoustic spectra of Piezo 1 (top row) and Piezo 2 (bottom row) for the four different color dye-water solutions as the target liquid analytes. As can be seen in figure 15, the PA spectra due to the transmitted and scattered light is uniquely different for different color dye-water solutions. In the spectra the first bar in white corresponds to the white LED, which is made of two wavelengths. All the rest of the bars corresponds to the PA amplitude by the LEDs with one particular wavelength in UV, visible and NIR region. If we focus on the visible region of the spectra in figure 15, we can quite easily find that the PA amplitude by the red LEDs is higher for red color dye-water solution. Similarly, in the visible region the green dye solution gives rise to a high value of the PA amplitude corresponding to the green LEDs. It demonstrates the discriminative capabilities of PA spectra of different color dyes. Also notice that the PA amplitudes at Piezo 2 is much higher than that of Piezo 1, because the dye-water solutions give rise to a higher scattering and the transmitted light is smaller than the scattered light. In next subsection 6.2, we will predict the concentration of a color dye in water. We will also have a more involved discussion on the relationship between the PA amplitude of Piezo 1 and Piezo 2 in section 6.2.

## 6.2 Predicting Color Dye Concentration in Dye-Water Solution

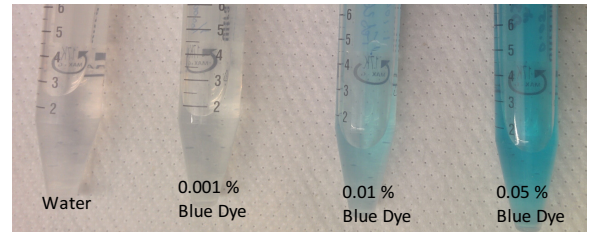


Figure 16: The 4 blue color dye solutions in water with concentrations of 0%, 0.05%, 0.01% and 0.0001%.

Whether our PA sensing system can predict or detect the concentration of a color dye was the next question that we asked in this study. We have prepared 4 different solutions by diluting blue color dye in water, as can be seen in figure 16. The concentration of the blue dye in these 4 solutions were respectively 0%, 0.001%, 0.01% and 0.05%.

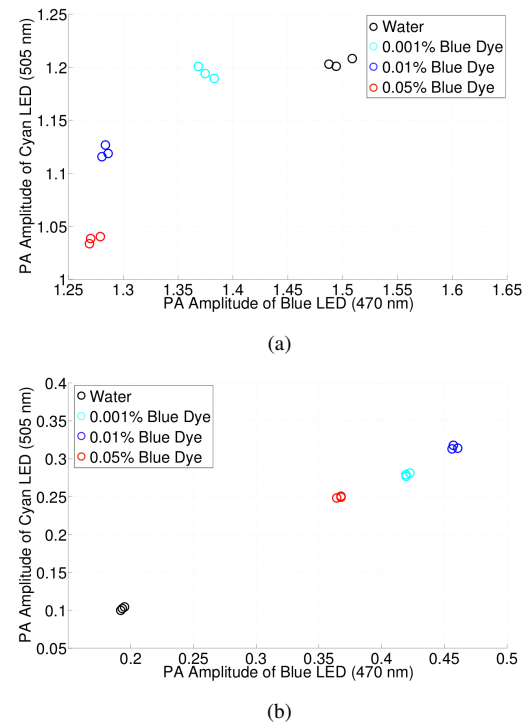


Figure 17: a scatter plot between the PA amplitudes of (a) Piezo 1 and (b) Piezo 2 by the Blue LED (center wavelength of 470 nm) and the Cyan LED (center wavelength of 505 nm).

We ran 3 independent trials with our system for each of these 4 analyte solutions. As blue colored LEDs can maximally pick up the change in concentration of blue color dye solutions, in figure 17 let us inspect the two scatter plots between PA amplitude of the blue LED (center wavelength of 470 nm) and the cyan LED (center wavelength of 505 nm). The subfigure 17a corresponds to the PA amplitudes of Piezo 1. As can be seen in the scatter plot 17a, with the increase in concentration of the solution, less blue light could pass through the solution in the cuvette and as a result less intensity modulated blue light beam reaches the surface of the piezoelectric sensor (Piezo 1). As more and more blue light gets reflected or scattered, it generates increasingly lower PA amplitude at the surface

of the brass piezoelectric sensor. Now if we inspect the subfigure 17b to analyze the scattered cyan and blue light's PA response at respectively 505 and 470 nm, we can observe that water or 0% blue dye generates the least amount of PA amplitude in Piezo 2. Water allows the light beam from both blue and cyan LED to pass without much (very little) scattering. As a result, the PA amplitude by the scattered light is also very small. We can also observe a significant increase in PA amplitude at Piezo 2 for 0.001% blue dye solution from the water. The added blue dye in water leads to a higher level of scattering which increases the PA amplitude at Piezo 2. Now, as we add even more blue dye to make the 0.05% blue dye solution, the PA amplitude of Piezo 2 by both LEDs decreases from that of 0.01%. The rationale behind this is that a much higher concentration of blue dye in water leads to higher reflection of blue light, which decreases the scattered light. These two scatter plot also shows that PA spectra of Piezo 1 and 2 contain complementary information about the target liquid analyte solution.

Now, leveraging the PA amplitudes of Piezo 1 and Piezo 2 by these two LEDs, we can predict the blue dye concentration in water. By training a neural network on the PA amplitude of these two LEDs only and then by running a leave-one-trial-out cross-validation experiment, we can reach a correlation coefficient of 0.9801, a mean absolute error of 3.54, a root mean square error of 4.29 and a root relative squared error of 14%. From this result, we can conclude that our system can characterize the color dye even with relatively very low concentrations.

## 7. CHARACTERIZING LIQUID FOOD AND DRINK WITH NUTRILYZER

In this section, we will present three feasibility experiments with Nutrilyzer in the context of liquid foods and drinks characterization. Firstly, we will illustrate how we can predict milk protein concentration. Secondly, we will discuss how we can detect a few different types of common milk adulterants with Nutrilyzer. Lastly, we explored if our system can potentially be used to characterize other liquid food and drink beyond milk such as alcohol.

### 7.1 Characterizing Milk Protein

Milk protein is one of the most important nutrients that is found in milk. In order to explore if our Nutrilyzer system can predict the concentration of protein in milk, we ran a feasibility experiment.

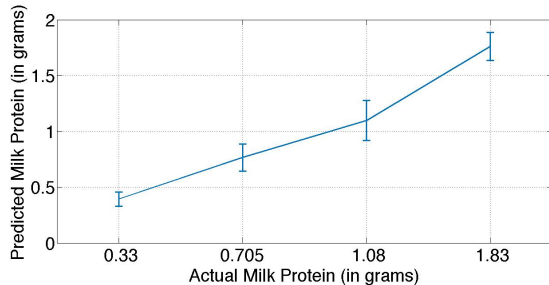


Figure 18: Milk protein concentration prediction in whole milk.

At first, we prepared 4 different milk solutions with 4 different amount of Milk Protein Concentrates (MPCs). MPC contain both casein and whey proteins in the same or similar ratio as milk [33]. As a result, MPC can emulate the protein that is found in milk. We started with whole milk, which contains 0.33 grams of milk protein in 10 ml of milk [9]. In order to vary the milk protein concentration, we have added 0.3750, 0.75 and 1.5 grams of MPC (by Idaho milk

product [7]) to 10 ml of whole milk. Thus we have prepared four 10 ml milk solutions with respectively 0.33, 0.705, 1.08 and 1.83 grams of milk protein.

Now, in order to test the predictability of milk protein concentrations, we ran 3 independent trials (by replacing the cuvette and the analyte solution) with each of the 4 milk solutions with our system. We used two PA spectra from both piezoelectric sensors to model a neural network to predict the amount of milk protein (in grams). From a leave-one-trial-out cross-validation, we found that with the PA spectra from both Piezos contains enough information to predict the milk protein in whole milk and the neural network achieved a Pearson correlation coefficient of 0.9063, a root mean squared error of 0.2468 and a root relative squared error of 16.7955%. The result shows that the proposed PAS system can successfully predict the milk protein concentration with a reasonable accuracy. Figure 18 illustrates a bar chart of the predicted milk protein (in grams) with respect to the actual amount. We can observe a linear relationship between the actual and predicted milk protein concentration (in grams per 10 ml). The neural network trained on the PA spectra could capture these 4 different milk protein concentration in whole milk with high confidence.

### 7.2 Characterizing Adulterants in Milk

Milk adulteration is a crucial problem in different parts of the world. As milk is a common ingredient for processing or preparing other foods and is more commonly consumed by the younger members of our society, adulteration of milk is a serious health hazard. As our second feasibility experiment, we explored if Nutrilyzer can detect and classify a few common milk adulterants. For this study, we considered four common milk adulterants: detergent, salt, starch, and water [40]. As can be seen in table 3, We have prepared 5 different Milk-Adulterant solutions in this experiment with the 4 type of adulterants. In 20 ml of whole milk, we have separately added 1.5 grams of starch, 1.5 grams of salt, 2 ml of liquid detergent and 2 ml of water. We have taken pure (100%) whole milk as baseline class.

| Milk-Adulterant Solution | Recipe                          |
|--------------------------|---------------------------------|
| Milk                     | 100% whole milk (no adulterant) |
| Milk + Detergent         | 2 ml in 20 ml milk              |
| Milk + Salt              | 1.5 grams in 20 ml milk         |
| Milk + Starch            | 1.5 grams in 20 ml milk         |
| Milk + Water             | 2 ml in 20 ml milk              |

Table 3: The list of the 5 different Milk-Adulterant solutions along with the recipes.

Now, in order to test the classifiability of these Milk-Adulterant solutions with our Nutrilyzer system, we ran 3 independent trials (by replacing the cuvette and the analyte solution) with each of the 5 milk solutions (as listed in table 3). In total, we have gathered photoacoustic spectral data from both piezoelectric transducers from 15 trials. The PA spectra is normalized by the spectra captured with an empty cuvette in the PA cell. We trained a neural network with the top feature subset selected by correlation-based feature selection (CFS) [23] and ran a leave-one-trial-out cross validation. The feature selection selected 4 features from the PA amplitude of Piezo 2. It is very interesting that for both milk protein concentration prediction and milk adulterant classification, most of the top selected features were PA amplitude of Piezo 2 at different wavelengths. Both adulterated and protein milk solutions are opaque and contain a lot of colloidal particles with different shape and size. Colloidal particles are typically much bigger in size, which is in the range of the wavelength that we considered in

this study (roughly). As the light travels the 10 mm path through the analyte milk solution, the colloidal particles scatter the light. This colloidal particle scattering is also known as Tyndall scattering [11]. Due to the heavy colloidal particle scattering, Piezo 2 gets a relatively stronger light beam, which gives rise to higher PA amplitude in Piezo 2. Due to the same reason, very little amount of low-intensity unscattered light can reach Piezo 1, which can only produce very small PA amplitude. The PA amplitude at Piezo 2 captures the characteristic colloidal particle scattering with a much higher signal to noise ratio than that of Piezo 1. As a result, the feature selection algorithm picked PA amplitudes at Piezo 2 as the top selected features.

Figure 19 demonstrates the scatter plot between two top selected features for milk adulterant classification: PA amplitude of Piezo 2 at 655 nm and PA amplitude of Piezo 2 at 448 nm. As can be seen in figure 19, all the classes are well separated except the milk with water slightly overlapping with salt. Also, notice that pure milk is distinctly far from all the adulterated liquid whole milk in figure 19, which shows that we can quite easily detect if the milk is adulterated or not. From a leave-one-trial-out cross-validation experiment with the top selected features trained neural network yields a performance of 80% recall and 78.5% of F-score when we try to classify among all the 5 classes including pure milk, milk with water, milk with salt, milk with starch, milk with detergent.

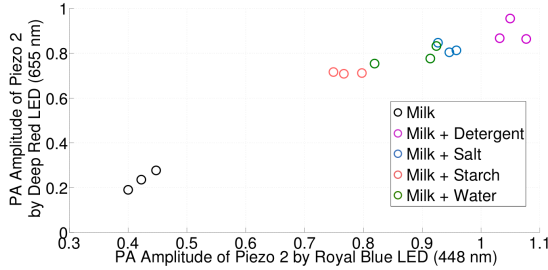


Figure 19: Scatter plot between two top discriminative features for milk adulterant classification.

### 7.3 Characterizing Alcohol Concentration

In this experiment, we explored if we can characterize the alcohol concentration in an alcoholic drink. In order to vary the alcohol concentration, we started from an alcoholic drink (Rum) with relatively high alcohol concentration (85%) and diluted the alcoholic drink (rum) with water. Thus we have prepared 6 different solutions with 100%, 80%, 60%, 40%, 20% Rum and water (0% Rum). Each solution was applied in the cuvette 3 times independently and we have gathered photoacoustic spectral data from 18 trials in total. All the PA spectra is normalized by the spectra captured with an empty cuvette in the PA cell. In order to model Rum concentration, we trained a neural network with the top feature subset selected by CFS feature selection [23] and ran a leave-one-trial-out cross validation. The feature selection selected both Piezo 1 and Piezo 2 PA amplitude. The top feature subset also includes the PA amplitude of Piezo 1 at 505 nm and Piezo 2 at 850 nm. In figure 20, you can visualize the error bars of the predicted Rum concentration with respect to the actual concentration. Our neural network achieves a Pearson correlation coefficient of 0.99, a mean absolute error of 2.01, an RMS error of 2.84 and a root relative squared error of 7.87%, which indicates that Nutrilyzer could capture the concentration of the alcoholic drink (Rum) with relatively high accuracy.

In addition to predicting the concentration of Rum, which is

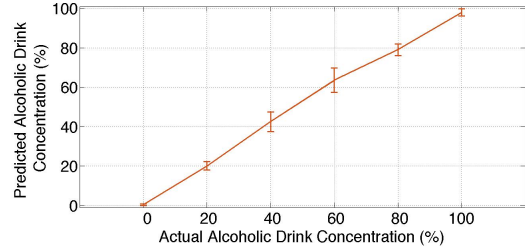


Figure 20: Predicting alcoholic drink (Rum) concentration in water.

slightly brownish in color, we also tried to predict the alcohol concentration of a clear (or colorless) alcoholic drink. As Rum has a brown color tone, the color tone will drop as it gets diluted in water. It has helped the regression model to achieve a good prediction. To answer this question, we have conducted another experiment with 95% clear alcohol, where we have again prepared 6 different solutions with 100%, 80%, 60%, 40%, 20% clear alcohol and water (0% clear alcohol). Each solution was applied in the cuvette 3 times independently and in total we have gathered photoacoustic spectral data from 18 trials. For clear alcohol concentration prediction, the top feature is selected to be the PA amplitude of Piezo 1 at 940 nm. Figure 21 shows the PA amplitude of Piezo 1 for all the different clear alcohol concentrations in water. As we add more clear alcohol to the water, the solution let more NIR light pass through it in the cuvette. As a result, more light hits the Piezo 1, which increases the PA amplitude. The performance of the neural network trained on the top features reaches a Pearson correlation coefficient of 0.91, a mean absolute error of 11.58, a RMS error of 15.23 and root relative squared error of 42.13%. Comparing the prediction result of the clear alcohol concentration prediction with the colored alcohol (Rum) concentration prediction, we can realize that the performance significantly dropped. This is due to the fact that our LED array does not capture various other wavelength in the near infrared and mid infrared regions which could be more beneficial for our system. In future by adding more LEDs with important wavelength, one could further boost the performance of the alcohol concentration prediction.

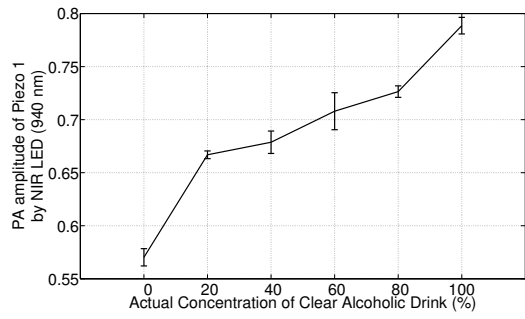


Figure 21: Near Infrared LED with center wavelength of 940 nm can capture the concentration of a clear alcoholic drink in water.

## 8. RELATED WORK

### 8.1 Photoacoustic Sensing Technique

The photoacoustic effect was an accidental discovery by Alexander Graham Bell in the year 1880 when he was experimenting

on long-distance sound transmission [16]. Around that time other physicists including John Tyndall and Wilhelm Röntgen also found this photoacoustic effect in gas [43, 36]. Alexander Graham Bell also demonstrated that with a rapidly interrupted beam of sunlight one could characterize solid sample material, even by the non-visible portion of the solar spectrum. However, the lack of highly sensitive acoustic sensor and wavelength tunable high power excitation source were the major bottlenecks towards widespread adoption of this technology. As the acoustic sensor and excitation source become respectively more sensitive and efficient, trace gas characterization was one of the first applications that used the photoacoustic effect [44, 39]. It is useful for substances in extremely low concentrations because very strong pulses of light from a laser can be used to increase sensitivity and very narrow bandwidth can be used for specificity. The first comprehensive theoretical description of the photoacoustic effect in solids was developed by Rosencwaig and Gersho in 1976 [38].

The piezoelectric sensor came into the realm of photoacoustic effect and spectroscopy, as it could directly capture the expansion and the compression of the photoacoustic effect directly from the target material. As a result, it obviates the need for an airtight, hermetically isolated photoacoustic chamber or cell. Another major advantage of the piezoelectric sensor is that it has a wide frequency response range (from a few Hz to many MHz), as a result, it can capture a broad range of photoacoustic temperatures and pressure wave. A detailed discussion on the piezoelectric sensor based photoacoustic effect can be found in [26, 45]. Piezoelectric photoacoustic effect has been used for characterizing solid [26, 34], liquid [29, 25] and gas [28].

## 8.2 Liquid Food Characterization

Photoacoustic sensing techniques have been explored for a wide variety of application scenario [42]. Especially, liquid material characterization using photoacoustic sensing has been studied in the context of different domain problems including biological system characterization [17], probing red blood cell morphology [41], and glucose testing [31]. Several recent studies used photoacoustic sensing technique to detect water pollution, such as Chromium contamination in water [30], trace oil detection in water [21]. A few recent studies also explore photoacoustic sensing techniques for liquid food characterization. Ravishankar and Jones used photoacoustic emission measurements to differentiate various liquid-based food and aqueous products [35]. This study has also modeled percentage of milk in water with photoacoustics. Milk and milk-based product have been extensively studied with photoacoustic spectroscopy using both UV and visible light [32]. The photoacoustic sensing technique was successful in predicting iron content in milk protein concentrate [19]. Milk adulteration was another interesting problem where the photoacoustic sensing technique was found to be useful. A recent study demonstrated that using the photoacoustic amplitude produced by visible range light could detect whey powder adulterant in skim milk [18]. In addition to the photoacoustic sensing, hyperspectral imaging is also proposed in the context of food characterization [22].

## 9. LIMITATIONS AND FUTURE WORK

Although Nutrilyzer shows great promise for mobile characterization of liquid foods and drinks, it is not without limitations. Although this paper has explored the feasibility of a photoacoustic effect based sensing system for milk and alcohol characterization, the potential generalizability of this approach for various other nutrient (or more generally chemical compounds) characterization of a wider variety of foods and drinks still remains an open question.

In other words, the question is how such a mobile system prototype like Nutrilyzer could potentially be extended for other types of liquid food or drink characterization. In order Nutrilyzer to detect other nutrients in some other type of liquid food or drink, we need to target the relatively unique part of the transmission or diffuse reflectance spectra and incorporate EM sources in that wavelength range. By incorporating more interesting and relevant wavelengths for a certain liquid food characterization problem, one could extend our system to other types of liquids. For example, for liquid alcohol concentration measurement, adding multiple EM sources between 1000 nm and 2400 nm could further boost the performance. One of the main bottlenecks of Nutrilyzer for achieving the generalizability to other types of liquids is rooted in the fact that we have only used a limited number of LEDs with certain wavelengths in UV, visible and shortwave NIR range. Unfortunately, the LEDs are not made at arbitrary wavelengths. The cost of a tunable laser is prohibitive to widespread adoption of such technology, which goes against the philosophy of making such a system mobile and ubiquitous. One way to tackle the problem could be to use optical filters in front of an LED to create various narrow bands. By capturing the PA amplitude at multiple interesting and relevant wavelengths could enable us to robustly capture subtle material attributes (e.g., concentration and material types) in other types of liquids.

Another interesting area for further exploration is improving the acoustic sensor. As future acoustic sensors will be even more sensitive, this will enable photoacoustic signal detection with a much higher SNR. We also plan to collect more data with various liquid foods in different settings to make the signal processing and prediction algorithm more robust. In the future, we plan to deploy our Nutrilyzer system in the wild in order to explore its applicability for low-cost liquid food characterization in the context of food safety and security.

## 10. CONCLUSION

In this paper, we have described the design, implementation, and evaluation of Nutrilyzer - a photoacoustic sensing system that can characterize various types of liquid food. Nutrilyzer uses an array of LED, two piezoelectric sensors and an ARM microcontroller unit to capture the photoacoustic signal of both the transmitted and scattered light beam in the target liquid food solution in a cuvette. The unique spectral signature captured by these two piezoelectric sensors across all the 16 LEDs in our LED array enable us to capture the optical transmission and scattering properties, which eventually leads us to detect nutrient and adulterants in liquid food. We have validated the feasibility of Nutrilyzer in three experiments with three different liquid foods. We demonstrated that we can predict the concentration of milk protein with a correlation coefficient of 0.90 and root relative squared error of 16%. We have also achieved 80% recall when we tried to classify various adulterants. With our limited number of LEDs in our LED array, we can quite easily predict the concentration of a colored alcohol (e.g., Rum with slightly brown tone) with a correlation coefficient of 0.99 and a root relative squared error of 7.87%. However, the performance drops significantly, when it comes to predicting clear alcohol concentration. In terms of correlation coefficient and root relative squared error the performance reaches respectively 0.91 and 42.13%.

## 11. ACKNOWLEDGMENTS

This work has been supported by the NSF CBET-1343058 grant. We are thankful for the valuable feedback from the reviewers and for the guidance of our shepherd Xiaofan Jiang.

## 12. REFERENCES

- [1] Brass piezoelectric disk sensor.  
<http://contactmicrophones.com/index.html>.
- [2] Cmos rail-to-rail op amp.  
<http://www.ti.com/product/TLV2772>.
- [3] luxeon rebel.  
<http://www.lumileds.com/uploads/20/DS63-pdf>.
- [4] Luxeon rebel and luxeon rebel es colors. http://www.lumileds.com/products/color-leds/luxeon-rebel-color.
- [5] luxeon z color line.  
<http://www.lumileds.com/uploads/415/DS105-pdf>.
- [6] luxeon z uv.  
<http://www.lumileds.com/uploads/441/DS114-pdf>.
- [7] Milk protein concentrate. <http://idahomilkproducts.com/product/milk-protein-concentrate-and-isolate-mpcmi>.
- [8] Picobuck, constant current led driver.  
<https://www.sparkfun.com/products/13705>.
- [9] Protein in whole milk. <https://en.wikipedia.org/wiki/Milk>.
- [10] Teensy 3.1 arm microcontroller.  
<https://www.pjrc.com/store/teensy31.html>.
- [11] Tyndall effect. [https://en.wikipedia.org/wiki/Tyndall\\_effect](https://en.wikipedia.org/wiki/Tyndall_effect).
- [12] Who technical report series on who diet, nutrition and the prevention of chronic diseases. <http://www.who.int/dietphysicalactivity/publications/trs916/summary>.
- [13] T. Allen and P. Beard. Light emitting diodes as an excitation source for biomedical photoacoustics. In *SPIE BioS*, pages 85811F–85811F. International Society for Optics and Photonics, 2013.
- [14] T. J. Allen and P. C. Beard. Pulsed near-infrared laser diode excitation system for biomedical photoacoustic imaging. *Optics letters*, 31(23):3462–3464, 2006.
- [15] A. G. Bell. Photoacoustic imaging and spectroscopy. *American Journal of Science*, 20(305), 1880.
- [16] A. G. Bell. Lxviii. upon the production of sound by radiant energy. *Philosophical Magazine Series*, 5(11):71, 1881.
- [17] M. Charland and R. M. Leblanc. Photoacoustic spectroscopy applied to biological systems (commemoration issue dedicated to professor tohru takenaka on the occasion of his retirement). 1993.
- [18] O. Dóka, D. Bicanic, and R. Frankhuizen. Photoacoustic study of heated binary mixtures containing whey and skimmed-milk powders. *Zeitschrift für Lebensmitteluntersuchung und-Forschung A*, 208(1):1–5, 1999.
- [19] O. Dóka, J. Kispéter, and A. Lörincz. Potential value of photoacoustic spectroscopy for determining iron content of milk protein concentrates. *Journal of dairy research*, 58(04):453–460, 1991.
- [20] D. I. Ellis, V. L. Brewster, W. B. Dunn, J. W. Allwood, A. P. Golovanov, and R. Goodacre. Fingerprinting food: current technologies for the detection of food adulteration and contamination. *Chemical Society Reviews*, 41(17):5706–5727, 2012.
- [21] N. Foster, J. Amonette, T. Autrey, and J. Ho. Detection of trace levels of water in oil by photoacoustic spectroscopy. *Sensors and Actuators B: Chemical*, 77(3):620–624, 2001.
- [22] M. Goel, E. Whitmire, A. Mariakakis, S. Saponas, N. Joshi, D. Morris, B. Guenter, M. Gavriliu, G. Borriello, and S. Patel. Hypercam: Hyperspectral imaging for ubiquitous computing applications. In *Proceedings of the 2015 ACM International Joint Conference on Pervasive and Ubiquitous Computing, UbiComp '15*, pages 145–156, 2015.
- [23] M. A. Hall. Correlation-based Feature Selection for Machine Learning. *PhD Thesis*, April 1999.
- [24] A. Hordvik and H. Schlossberg. Photoacoustic technique for determining optical absorption coefficients in solids. *Applied optics*, 16(1):101–107, 1977.
- [25] T. Ikari, H. Matsuyama, A. Nakashima, and K. Futagami. Piezoelectric photoacoustic spectra of silicon at liquid helium temperature. In *Ultrasonics Symposium, 1994. Proceedings., 1994 IEEE*, volume 2, pages 737–740. IEEE, 1994.
- [26] W. Jackson and N. M. Amer. Piezoelectric photoacoustic detection: theory and experiment. *Journal of Applied Physics*, 51(6):3343–3353, 1980.
- [27] R. G. Kolkman, W. Steenbergen, and T. G. van Leeuwen. In vivo photoacoustic imaging of blood vessels with a pulsed laser diode. *Lasers in medical science*, 21(3):134–139, 2006.
- [28] N. Ledermann, J. Baborowski, A. Seifert, B. Willing, S. Hiboux, P. Muralt, N. Setter, and M. Forster. Piezoelectric cantilever microphone for photoacoustic gas detector. *Integrated Ferroelectrics*, 35(1-4):177–184, 2001.
- [29] W. P. Leung and A. C. Tam. Noncontact monitoring of laser ablation using a miniature piezoelectric probe to detect photoacoustic pulses in air. *Applied physics letters*, 60(1):23–25, 1992.
- [30] J. Lima, E. Marin, S. Cardoso, O. Delgado-Vasallo, M. d. SILVA, M. Sthel, C. Gatts, A. Mariano, C. Rezende, A. Ovalle, et al. Application of novel photoacoustic measurement designs to chromium (vi) determination in water. *Analytical Sciences/Supplements*, 17(0):s530–s533, 2002.
- [31] H. A. MacKenzie, H. S. Ashton, S. Spiers, Y. Shen, S. S. Freeborn, J. Hannigan, J. Lindberg, and P. Rae. Advances in photoacoustic noninvasive glucose testing. *Clinical Chemistry*, 45(9):1587–1595, 1999.
- [32] R. Martel, C. N. N'Soukpoé-Kossi, P. Paquin, and R. M. Leblanc. Photoacoustic analysis of some milk products in ultraviolet and visible light. *Journal of dairy science*, 70(9):1822–1827, 1987.
- [33] H. P. Patel and S. Patel. Milk protein concentrates: Manufacturing and applications. *Technical Report*.
- [34] M. D. Rabasović, M. G. Nikolić, M. D. Dramićanin, M. Franko, and D. D. Markushev. Low-cost, portable photoacoustic setup for solid samples. *Measurement Science and Technology*, 20(9):095902, 2009.
- [35] S. Ravishankar and B. Jones. Photo-acoustic emission measurements in liquid-based food.
- [36] W. C. Röntgen. On tones produced by the intermittent irradiation of a gas. 1881.
- [37] A. Rosencwaig. Photoacoustic spectroscopy of solids. *Optics Communications*, 7(4):305–308, 1973.
- [38] A. Rosencwaig and A. Gershoff. Theory of the photoacoustic effect with solids. *Journal of Applied Physics*, 47(1):64–69, 1976.
- [39] S. Schäfer, A. Miklós, A. Pusel, and P. Hess. Absolute measurement of gas concentrations and saturation behavior in pulsed photoacoustics. *Chemical physics letters*, 285(3):235–239, 1998.
- [40] H. Singuluri and M. Sukumaran. Milk adulteration in hyderabad, india: A comparative study on the levels of different adulterants present in milk. *Journal of Chromatography & Separation Techniques*, 2014, 2014.

- [41] E. M. Strohm, E. S. Berndl, and M. C. Kolios. Probing red blood cell morphology using high-frequency photoacoustics. *Biophysical journal*, 105(1):59–67, 2013.
- [42] A. C. Tam. Applications of photoacoustic sensing techniques. *Reviews of Modern Physics*, 58(2):381, 1986.
- [43] J. Tyndall. Action of an intermittent beam of radiant heat upon gaseous matter. *Proceedings of the Royal Society of London*, 31(206-211):307–317, 1880.
- [44] M. Viengerov. New method of gas analysis based on tyndall-roentgen optoacoustic effect. *Doklady Akademii Nauk SSSR*, 19(687):8, 1938.
- [45] G. C. Wetsel Jr. Photoacoustic effect in piezoelectric ceramics. *JOSA*, 70(5):471–474, 1980.